

# From stationary to complex time-dependent flows at moderate Rayleigh numbers in two-dimensional annular thermal convection

Marta Net, Arantxa Alonso, and Juan Sánchez

*Departament de Física Aplicada, Universitat Politècnica de Catalunya, Mòdul B4, Campus Nord, 08034 Barcelona, Spain*

(Received 9 May 2002; accepted 7 February 2003; published 4 April 2003)

Two-dimensional nonlinear thermal convection in a cylindrical annulus is numerically analyzed for a Boussinesq fluid of low Prandtl number  $\sigma=0.025$ . For a fixed value of the radius ratio,  $\eta=0.3$ , different types of steady columnar patterns are found. The stability of these convection patterns and the spatial interaction between them, which result in the formation of mixed modes, are investigated by considering the full nonlinear set of Navier–Stokes equations. Special attention is paid to the strong spatial interaction of the initially unstable modes with wavenumbers  $n=2$  and  $n=4$ , which leads, through global bifurcations, to multiple stable quasi-periodic states of the system. A detailed picture of the nonlinear dynamics until temporal chaotic patterns set in is presented and understood in terms of local and global symmetry-breaking bifurcations of the  $O(2)$ -symmetric system. © 2003 American Institute of Physics. [DOI: 10.1063/1.1565335]

## I. INTRODUCTION

The large-scale azimuthal motions in the atmospheres of major planets and in planetary fluid cores have in common the influence of the spherical geometry, which makes the relative orientation of gravity and rotation vectors vary with latitude, and the strong effect of high Taylor numbers. Since it is impossible to reproduce such convective systems in terrestrial laboratory experiments, due to the presence of vertical gravity and the difficulties of producing a radial gravity, these flows have given rise to studies of thermal convection in cylindrical annular geometries with radial inwards heating and the radial gravity emulated by the centrifugal buoyancy. The experimental results<sup>1,2</sup> showed that the constraint of large Taylor numbers causes the motion to remain nearly two-dimensional, with departures from two-dimensionality confined to narrow Ekman layers at the ends of the annulus. Consequently, some subsequent theoretical and numerical papers<sup>3–7</sup> are based on this fact and look for axial-independent solutions in the narrow gap limit. Others<sup>8–10</sup> are direct numerical simulations allowing the imposition of a radial constant inwards gravity changing the sign of the temperature gradient. They can capture the same nonlinear dynamics, because, except for the geometry and the definition of the Rayleigh number, they obtain equivalent nondimensional equations. Considering a constant or a radial dependent gravity vector does not affect the radial symmetries of the problem unless the narrow gap approximation ( $\eta \rightarrow 1$ ) is made. In this case the problem may gain an additional mid-plane symmetry depending on the curvature of the top and bottom boundaries.

A three-dimensional rotating annulus, with either top and bottom horizontal or inclined lids, is invariant under rotations about the rotation axis, i.e., their symmetry group in the azimuthal direction is  $SO(2)$ . A symmetry-breaking bifurcation of an axisymmetric state (like conduction) must be a

Hopf bifurcation,<sup>11</sup> which gives rise to waves traveling in the azimuthal direction. Rigorously, any approximation of the three-dimensional problem must keep the symmetries of the original one, otherwise the spatio-temporal dynamics can change from the first bifurcation. This is what happens if the two-dimensional annular geometry is taken for approximating the azimuthal waves of a slow rotating annulus with no-slip top and bottom lids. By introducing the streamfunction formulation the rotation drops out<sup>12</sup> and the equations can be written in the form of a two-dimensional Rayleigh–Bénard problem without the midplane layer symmetry, i.e., the problem recovers the reflection symmetry in vertical planes through the axis of rotation, and the  $O(2)$  symmetry forces a primary stationary bifurcation. An easy way of achieving the  $SO(2)$  symmetry of the complete three-dimensional problem in a  $z$ -independent problem is to consider the quasi-geostrophic solutions of the fast rotating annulus with slightly inclined top and bottom lids.<sup>3</sup> In the resulting two-dimensional equations, the  $\beta$  term breaks the preceding reflection symmetry in vertical planes. As a result, the primary convective solutions are azimuthal drifting waves (thermal Rossby waves), which give rise to secondary nonlinear patterns dominated by the Coriolis term and the vortex stretching due to the topographic  $\beta$  effect.

In the fast rotation limit, it is easy to see, by comparison of Refs. 13, 14, and 9, that the  $(r, \theta)$  dependence and frequency of the waves is different depending on the type of top and bottom lids. The linear stability analysis of the conduction state of a rotating annulus with radial gravity, outwards<sup>14</sup> or internal heating<sup>13</sup> and experimental no-slip boundary conditions on the horizontal top and bottom lids, shows that, for Taylor numbers  $Ta > 10^6$ , the convection is already nearly two-dimensional, with departures from two-dimensionality confined to narrow Ekman layers at the ends of the annulus. With  $Ta > 10^6$ , for a fluid of  $\sigma=0.025$  in an annulus of radius ratio  $\eta=0.35$  and aspect ratio  $\beta=1$  (defined in Sec. II), the

precession frequency, in viscous units, is smaller than  $\omega = 0.08$ , i.e., several orders of magnitude smaller than that found for the thermal inertial waves of the slanted lids,<sup>9</sup> and unlikely to be measurable in a laboratory experiment. The linear modes that first become unstable are determined physically by the balance among the terms of the linear system. For example, for small Prandtl numbers with slanted lids, the balance is mainly established between the large inertial term and the  $\beta$  term, the buoyancy force playing a secondary role. However, with horizontal lids, the precession frequency tends to zero as the Taylor number tends to infinity, and the buoyancy force contributes at first order to the linear balance. Therefore, the physical nature of the primary instability is basically inertial or thermal depending on the geometry.

Thermal steady columns are exact solutions of the fast rotating annulus with stress-free boundary conditions on the flat lids.<sup>12,15</sup> In fact, they coincide with the two-dimensional vortices of the plane geometry. In the no-slip case, the numerical results<sup>14</sup> and also the asymptotic theory<sup>13</sup> show that the influence of the Ekman boundary layers decreases as the aspect ratio increases. At leading order,  $Ra_c = Ra_0 - CT^{1/4}/\beta$  and  $\omega = 0$ , where  $Ra_0$  is the critical Rayleigh number when  $\beta \rightarrow \infty$ , i.e., it is the Rayleigh number of the thermal columns. The constant  $C$  is independent of the Prandtl number. On the other hand, for large aspect ratios, the contour plots of the temperature or the velocity field, with both boundary conditions, only differ in the very narrow top and bottom boundaries. Therefore, the primary convective flow almost recovers the reflection symmetry of the thermal columns. In addition, the experimental results and the linear asymptotic analysis<sup>3</sup> in fast rotating systems indicate that from low to moderate Rayleigh numbers the Ekman layers remain attached to the lids when the full nonlinear dynamics is developed. Under these conditions, and taking into account that the type of bifurcations of a solution depends on its symmetries, the question is; up to what point is it possible to approximate the nonlinear evolution of the *almost* thermal columns by a  $z$ -independent problem? In order to answer this question, we study numerically the influence of the  $O(2)$  symmetry on the convection driven by radial gravity and heating, specifically on the nonlinear dynamics of the two-dimensional thermal columns. A summary of the sequence of bifurcations and information about the symmetries of the solutions, up to the onset of preturbulent flows, are presented.

This study has been focused on  $\sigma = 0.025$  (mercury) and a radius ratio  $\eta = 0.3$ . Metallic liquids are fluids of primary geophysical and magnetohydrodynamics interest. They are difficult to handle in laboratory experiments, since their internal structures cannot be directly observed. Numerical experiments with low Prandtl number fluids furnish information that would be hard to obtain in laboratory conditions. On the other hand, with small  $\eta$ , a dynamics dominated by the spatial 1:2 resonance might be expected *a priori*. In effect, the analysis of a long-wave model for two-dimensional convection in a plane layer shows that the 1:2 resonance is dominant when asymmetric boundary conditions are considered.<sup>16</sup> In two-dimensional Rayleigh–Bénard convection, the same effect can be achieved by considering different

boundary conditions at top and bottom or by including non-Boussinesq terms.<sup>17</sup> With symmetric boundary conditions, the leading order resonant term in the 1:2 interaction is of higher order than that in the 1:3 interaction.<sup>16,18</sup> In addition, both values of the parameters allow us to compare the linear primary modes and critical parameters of convection for any of the above-mentioned problems.

The type of bifurcation that a solution which has broken the rotation symmetry but keeps the reflection symmetry may undergo is known, but subsequent bifurcations remain unclear. If the azimuthal structure of the flow is maintained, according to bifurcation theory,<sup>19,20</sup> it can suffer four possible codimension one bifurcations depending on the parameters of the system. The new solution can either keep the reflection symmetry of the basic solution or break it. In the first case, the bifurcation can be a saddle-node or a Hopf bifurcation that gives rise to a standing wave without any spatial drift. In the second case, it can either be a pitchfork or a Hopf bifurcation, leading to traveling waves, which have a drift speed that increases with increasing the bifurcation parameter, or to direction reversing traveling waves (DRTW) that are vacillating waves, which alternatively drift back and forth.<sup>21</sup> The parameters we have employed give way to the last kind of bifurcation. Obviously, by changing these parameters, the thermal columns could undergo any of the other bifurcations and a different dynamics than that described in this paper would be observed.

The nonlinear dynamics of the two-dimensional columns also provides a simple fluid dynamics system which is highly attractive from the point of view of bifurcation theory, because it is large enough to provide a rich spatio-temporal dynamics induced by the reflection symmetry in vertical planes, but at the same time not as expensive in calculation time as a three-dimensional system. In this context, our results can be relevant to any problem that shares the same symmetries. This is the case of electroconvection in an annular suspended film, where radial driving forces are the experimental conditions. Unfortunately, it is not possible to establish a direct comparison because the experiments<sup>22,23</sup> are mainly carried out with a rotating inner electrode and, as in the rotating annulus, the reflection symmetry of the system is broken.

The paper is organized as follows. In Sec. II we introduce two different formulations of the problem and the numerical methods used to solve it. In Sec. III we analyze the stability and interaction of the steady solutions that bifurcate from the conduction state, which leads to the stabilization of the flow and to global bifurcations. In Sec. IV the time-dependent behavior of the stable flows that coexist in a wide range of Rayleigh numbers is studied. New complex flows are presented consisting of random switching between reflection symmetric quasi-periodic solutions, and gluing bifurcations of tori, also induced by the reflection symmetry of the system. Finally, Sec. V includes a summary of the results and the main conclusions.

## II. BASIC EQUATIONS

We consider an annulus which is rotating about its axis of symmetry with angular velocity  $\Omega$ . The gap width is  $d$

$\equiv r_o - r_i$ , where  $r_i$  and  $r_o$  are the inner and outer radii, and  $L$  is the height of the layer. The geometric parameters of the problem are the radius ratio  $\eta \equiv r_i/r_o$  and the aspect ratio  $\beta \equiv L/d$ . The inner and outer side walls are maintained at constant temperatures  $T_i$  and  $T_o$ , respectively, with  $T_i > T_o$ , and for the velocity field no-slip lateral boundary conditions

$$u = v = w = 0 \quad \text{on } r = r_i, r_o, \quad (1)$$

are taken.

As we have already mentioned in Sec. I, the present study will focus on the nonlinear analysis of the  $z$ -independent columnar solutions, which are exact solutions of the problem in the stress-free lids case. We write the two-dimensional Boussinesq Navier–Stokes, mass conservation, and energy equations in the rotating frame of reference, and we consider a constant gravity across the convective layer,  $g$ , which is also assumed to be radially inwards. We also assume that  $r\Omega^2/g \ll 1$ , a condition that can be accomplished, for instance, in planetary cores. To nondimensionalize the equations we use the gap width, the temperature difference between the side boundaries and the thermal diffusion time  $d^2/\kappa$ , where  $\kappa$  represents the thermal diffusivity. The problem is formulated in terms of both the velocity–pressure and the streamfunction formulation. In the latter case, we define a new pressure modified by the Coriolis term and we write the velocity field as

$$\mathbf{u} = f\hat{\mathbf{e}}_\theta + \nabla \times (\psi\hat{\mathbf{e}}_z), \quad (2)$$

where  $f(r)$  is needed to guarantee the possible existence of an azimuthal mean flow, if the azimuthal average of  $\psi(r, \theta)$  is imposed to be zero by the homogeneous boundary conditions. The equations for  $f$ ,  $\psi$ , and the departure from the conductive state temperature,  $\Theta$ , are

$$(\partial_t - \sigma\tilde{\Delta})f = P_\theta \left[ \Delta\psi \left( \frac{1}{r} \partial_\theta \psi \right) \right], \quad (3a)$$

$$\begin{aligned} (\partial_t - \sigma\Delta)\Delta\psi = & \frac{\sigma\text{Ra}}{r} \partial_\theta \Theta + (1 - P_\theta)J(\psi, \Delta\psi) \\ & + \tilde{\Delta}f \left( \frac{1}{r} \partial_\theta \psi \right) - f \left( \frac{1}{r} \partial_\theta \Delta\psi \right), \end{aligned} \quad (3b)$$

$$(\partial_t - \Delta)\Theta = -\frac{1}{r^2 \ln \eta} \partial_\theta \psi + J(\psi, \Theta) - f \left( \frac{1}{r} \partial_\theta \Theta \right), \quad (3c)$$

where  $\tilde{\Delta} = \partial_r(\partial_r + 1/r)$ .  $P_\theta$  is the operator that averages in the azimuthal direction and  $J$  is the determinant of the corresponding Jacobian matrix in cylindrical coordinates. The nondimensional parameters that appear in the equations are the Rayleigh and Prandtl numbers defined by

$$\text{Ra} \equiv \frac{\alpha \Delta T g d^3}{\kappa \nu}, \quad \sigma \equiv \frac{\nu}{\kappa}.$$

The Taylor number does not appear in the equations because we are looking for columnar solutions.

The boundary conditions are now

$$f = \psi = \partial_r \psi = \Theta = 0 \quad \text{on } r = r_i, r_o. \quad (4)$$

TABLE I. Comparison of the frequencies of a quasi-periodic solution at  $\text{Ra} = 20\,000$ . VP and SF refer, respectively, to the velocity–pressure and the streamfunction codes.  $LL$  and  $N$  are, respectively, the radial and azimuthal resolutions.

Code	$LL \times N$	$f_1$	$f_2$
VP	$32 \times 192$	9.567	0.412
VP	$32 \times 256$	9.567	0.412
VP	$48 \times 192$	9.567	0.412
SF	$32 \times 192$	9.566	0.397
SF	$32 \times 256$	9.566	0.397

These equations are solved numerically using two different continuation codes to find the steady solutions, and semi-implicit backward differentiation formulas–extrapolation time-stepping codes for the time-dependent solutions. We have used a time-splitting code, written in terms of the velocity field,  $(u, v)$ , and, to be sure that the solutions are not spurious, a streamfunction code, with checked integration methods up to fourth order in time. The method to evaluate linear and nonlinear terms is different in each case. The variables are always expanded in terms of Chebyshev polynomials  $T_l$ , and Fourier expansions. For the streamfunction formulation they are

$$f(x, t) = \sum_l \alpha_l(t) T_l(x), \quad (5a)$$

$$\psi(x, \theta, t) = \sum_{l, n} \gamma_{ln}(t) T_l(x) e^{in\theta}, \quad (5b)$$

$$\Theta(x, \theta, t) = \sum_{l, n} \delta_{ln}(t) T_l(x) e^{in\theta}. \quad (5c)$$

The radial coordinate is  $x = 2r - \delta$ , with  $\delta = (1 + \eta)/(1 - \eta)$ , and the integers  $(l, n)$  indicate the structure of the functions in the radial and azimuthal directions, respectively. The coefficients  $\alpha_l$ ,  $\gamma_{ln}$ , and  $\delta_{ln}$  are related by the boundary conditions. In the  $(u, v)$  formulation, the mean flow is directly the  $n = 0$  mode of  $v$ .

Some proofs have been made to determine the numerical resolution needed in our calculations. A test of the dependence of the frequencies of a quasi-periodic solution for  $\text{Ra} = 20\,000$  is presented in Table I. A tiny difference of 0.01% in the main frequency  $f_1$  is found, but the difference increases up to 4% for the small frequency  $f_2$ , when the time integration method is changed. We believe that this is due to the higher temporal order of the integrator used in the streamfunction formulation, which allows a better determination of the small frequencies. Thus, for the solutions with  $\text{Ra} > 7000$ ,  $32 \times 192$  radial by azimuthal points are used. In general, for  $\text{Ra} < 7000$ , the steady columns and their stability are calculated with  $24 \times 192$  points. The bifurcations corresponding to high Rayleigh numbers are transitions between time complex regimes that cannot be determined precisely with only time evolution codes. The exponential decay (or growth) of the solutions near a bifurcation point is too slow and, in addition, different with the two time evolution orders employed. Even with these difficulties we have found only differences below a 0.5% in the determination of the transitions at  $\text{Ra} > 18\,000$ .

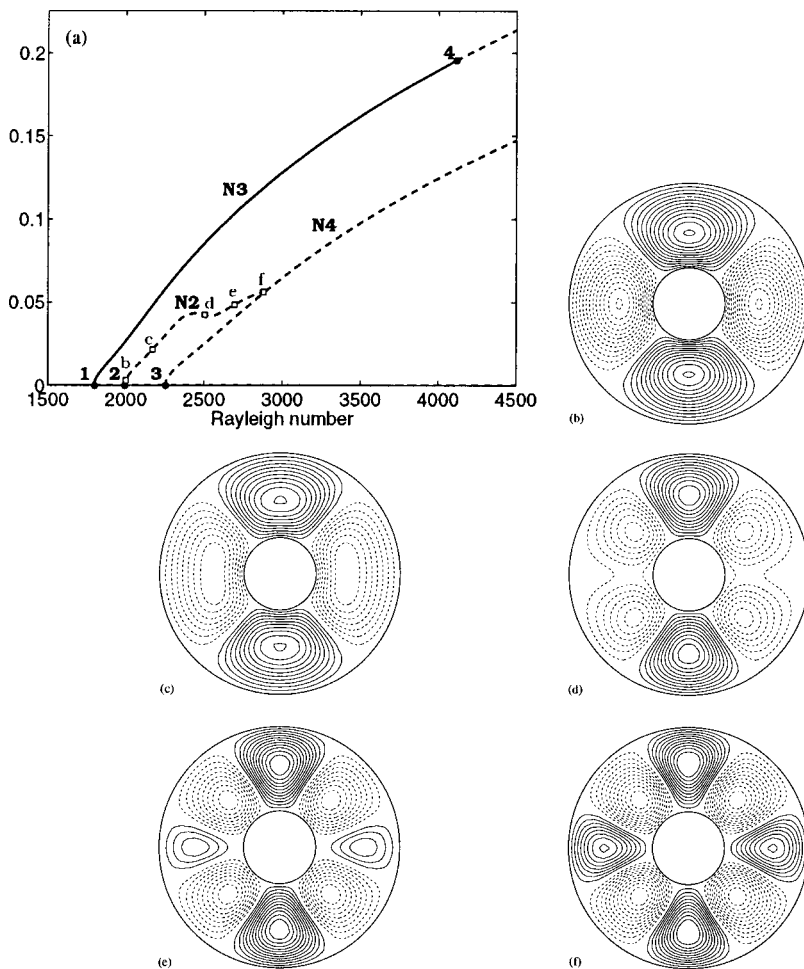


FIG. 1. (a) Bifurcation diagram showing branches of columnar modes with wavenumbers  $n=3$ ,  $n=2$ , and  $n=4$  ( $N3$ ,  $N2$ , and  $N4$  branches, respectively). They arise at  $Ra_c^1=1799$  (1),  $Ra_c^2=1995$  (2), and  $Ra_c^3=2254$  (3). (b)–(f) The contour plots of the temperature perturbation showing the structure of the solutions in the  $N2$  branch, corresponding to the points  $b$  ( $Ra=2000$ ),  $c$  ( $Ra=2198$ ),  $d$  ( $Ra=2500$ ),  $e$  ( $Ra=2711$ ), and  $f$  ( $Ra=2875$ ) in the diagram, respectively.

Throughout the paper, the Nusselt number, defined as a measure of the radial heat transport by convection, has been computed in the outer cylinder as

$$Nu = 1 + \frac{\ln \eta}{1 - \eta} \int_0^{2\pi} \partial_r \Theta(1, \theta, t) d\theta. \tag{6}$$

### III. STEADY STATE THERMAL COLUMNS

In this section we describe the steady columnar patterns that bifurcate from the conduction state, and analyze their stability and symmetries in order to understand the global nonlinear dynamics described in Sec. IV. We will show the importance of including the study of the unstable branches in order to fully capture the stable dynamics of the system.

Some preliminary results have already been published,<sup>24,25</sup> but are included because they are closely related with the new solutions presented in this paper. As a first step, we have carefully checked that the continuation and time-integration codes reproduce accurately the onset of convection and agree for the nonlinear solutions. The diagram of Fig. 1(a) shows the branches of columnar solutions with basic azimuthal wavenumbers  $n=3, 2, 4$  ( $N3$ ,  $N2$  and  $N4$  branches, respectively). We display  $\sqrt{\sum_n \delta_{ln} \delta_{ln}^*}$  for a fixed radial amplitude  $l$ ,  $\delta_{ln}^*$  being the conjugate of  $\delta_{ln}$ . The axisymmetric conduction state becomes unstable to columns with wavenumber  $n=3$  at  $Ra_c^1=1799$  (point 1 in the bifur-

cation diagram), in agreement with the wavenumber predicted by the linear stability analysis. For slightly larger Rayleigh numbers, the conduction state is also unstable to modes with wavenumbers  $n=2$  (at  $Ra_c^2=1995$ ) and  $n=4$  (at  $Ra_c^3=2254$ ). All these new nonaxisymmetric solutions break the rotation symmetry,  $R_\theta$ , of the basic state, but maintain the reflection symmetry,  $R$ , with respect to appropriate vertical planes  $\theta=\theta_0$ , and the invariance under  $2\pi/n$ -rotations,  $R_{2\pi/n}$ , i.e.,

$$\Theta(x, \theta) = \Theta(x, 2\theta_0 - \theta), \quad \psi(x, \theta) = -\psi(x, 2\theta_0 - \theta), \tag{7a}$$

$$\Theta(x, \theta) = \Theta(x, \theta + 2\pi/n), \quad \psi(x, \theta) = \psi(x, \theta + 2\pi/n). \tag{7b}$$

The discrete group of symmetry of the new solutions is  $D_n$ . Bifurcations from the conduction state are symmetry-breaking steady-state bifurcations in which multiplicity two eigenvalues cross the imaginary axis.

While solutions along the  $N3$  and  $N4$  branches are pure modes, in which only the basic wavenumbers and their harmonics are nonzero, the  $N2$  is a mixed-mode branch. There is a strong spatial interaction between the  $n=2$  and  $n=4$  modes (spatial 1:2 resonance), which produces a change in the structure of the solution along the  $N2$  branch. To illustrate the physical nature of these solutions, the contour plots of the perturbation of the temperature at different Rayleigh

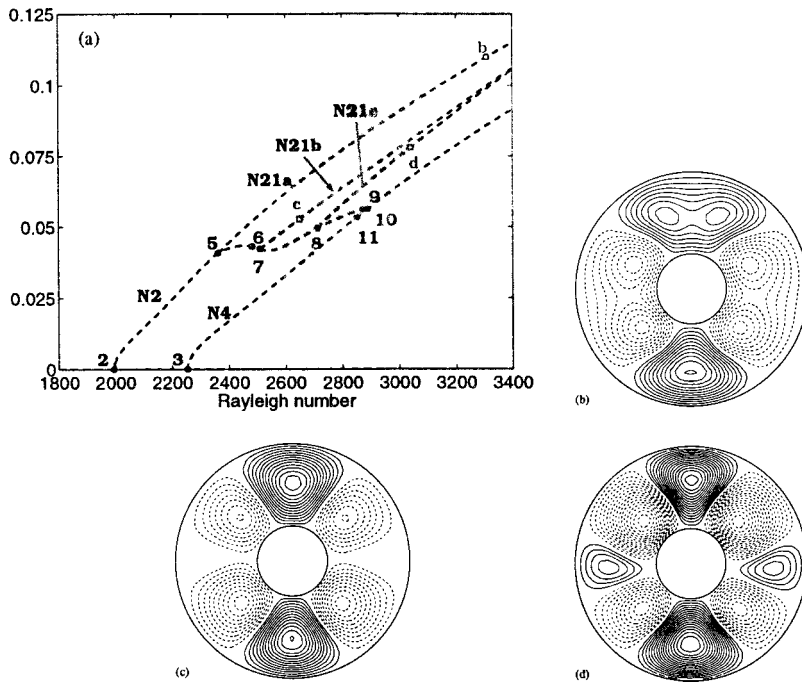


FIG. 2. (a) Detail of the steady-state bifurcations on the  $N2$  and  $N4$  branches, which take place at  $Ra_c^5=2362$  (5),  $Ra_c^6=2478$  (6),  $Ra_c^7=2509$  (7),  $Ra_c^8=2712$  (8),  $Ra_c^9=2887.5$  (9), and  $Ra_c^{10}=2888.9$  (10) on the  $N2$  branch and at  $Ra_c^{11}=2851$  (11) and  $Ra_c^{10}=2888.9$  (10) on the  $N4$  branch. (b), (c), (d) The contour plots of the temperature perturbation showing the structure of the solutions in the  $N21a$ ,  $N21b$  and  $N21c$  branches, corresponding to points  $b$  ( $Ra=3308$ ),  $c$  ( $Ra=2649$ ), and  $d$  ( $Ra=3040$ ) of the bifurcation diagram, respectively.

numbers are shown from Figs. 1(b)–1(f). As the Rayleigh number increases, the contribution of the  $n=4$  mode becomes more important, while the  $n=2$  contribution diminishes until vanishing. The initial two pairs of rolls become an  $n=4$  solution.

A stability analysis of the mixed-mode solutions shows that there are several bifurcations in the  $N2$  branch. The new branches, which we have been able to follow with the continuation code, are included in Fig. 2(a). Bifurcation points 5 ( $Ra_c^5=2362$ ), 7 ( $Ra_c^7=2509$ ), and 8 ( $Ra_c^8=2712$ ) correspond to subharmonic steady-state bifurcations. The solutions in these new branches, which are displayed in Figs. 2(b)–2(d), still keep the reflection symmetry, but now there is a contribution of all the wavenumbers. Their symmetry group is  $Z_2$ , generated by a reflection, defined as in Eq. (7a), through the  $\theta_0 \approx \pi/2$  plane in the figures. The bifurcation identified in point 6 ( $Ra_c^6=2478$ ) corresponds to a steady-state instability that keeps the wavenumber of the main solution,  $n=2$ , but in which the mean flow becomes nonzero. According to bifurcation theory,<sup>20</sup> a steady-state bifurcation that breaks the reflection symmetry, keeping the discrete rotational invariance, would give rise to traveling waves with zero phase speed at the bifurcation point. Nevertheless, we have not followed this time-dependent branch which, in our case, is unstable. Finally, two subsequent bifurcations very close to each other occur at points 9 and 10. At the first ( $Ra_c^9=2887.5$ ), one of the two positive eigenvalues of the solution is stabilized through a subharmonic steady-state bifurcation. At the second ( $Ra_c^{10}=2888.9$ ), the amplitude of the  $n=2$  mode vanishes. The  $N2$  branch joins the  $N4$  branch, and columns with wavenumber  $n=2$  cease to exist. This is a bifurcation from the  $N4$  branch, which occurs after a bifurcation in  $Ra_c^{11}=2851$  at which an eigenvalue with multiplicity two gains stability.

All the above-described steady patterns, except for the

$n=3$  column, are unstable. However, by extending further the  $N4$  branch, a bifurcation that stabilizes the pure  $n=4$  solution by shedding a new unstable branch takes place at  $Ra_c^{12}=4779$  (not shown in the figures). Later bifurcations connected with this branch give rise to pairs of quasi-periodic flows related by the reflection symmetry.

#### IV. TIME-DEPENDENT SOLUTIONS

In this section we will describe the nonlinear solutions found by increasing the Rayleigh number, when the steady columns lose stability. The symmetry of the solutions is analyzed in order to understand the influence of the  $O(2)$  symmetry at moderate Rayleigh numbers. First of all, the sequence of local bifurcations and time-dependent solutions with basic azimuthal wavenumber  $n=3$  are considered in Sec. IV A. Section IV B is devoted to the study of the time-dependent flows, which arise near the strong 1:2 spatial resonance. It will be seen that the  $n=4$  steady flow bifurcates to a DRTW, which in terms of the bifurcation theory is a symmetric cycle. For these time-dependent solutions, the evolution by half a period in time is equivalent to acting by the reflection that is broken in the bifurcation. Via local transitions that consecutively break all the symmetries of the periodic orbits, pairs of quasi-periodic solutions related through the reflection symmetry in vertical planes are found. We will call these solutions  $R$ -conjugate tori because by applying the reflection symmetry to one of them, the other is obtained. Ultimately, global bifurcations of the quasi-periodic solutions restore the reflection symmetry in the sense that if the reflection symmetry is applied to the new solutions (quasi-periodic or not), at any instant of time, another point of the same solution, at a different time, is obtained ( $R$ -invariant

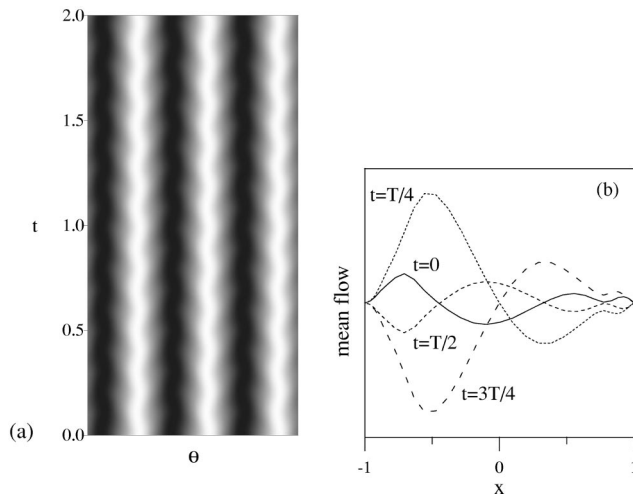


FIG. 3. Pure  $n=3$  direction reversing traveling wave. (a) Shadowgraph showing the evolution of the temperature perturbation in time at the radial midpoint of the annulus, for a solution corresponding to  $Ra=5000$ . (b) Four snapshots showing the radial dependence of the azimuthal mean flow.

solutions). Finally, for a complete description of the spatio-temporal dynamics, an additional branch of mixed solutions is included in Sec. IV C.

To facilitate the reading of the paper, the results are summarized in a schematic bifurcation diagram (Fig. 14) in the final discussion of the paper.

### A. Nonlinear solutions with basic dominant wavenumber $n=3$

The linear stability analysis of the  $N3$  branch of solutions shows that there is a secondary Hopf bifurcation at  $Ra_c^4=4114$ , the imaginary part of the critical eigenvalues being  $\lambda_I = \pm 23.5$ . It corresponds to point 4 of Fig. 1(a). The nonlinear steady columns become unstable and they give rise to DRTW, which keep the same basic azimuthal wavenumber of the steady  $n=3$  columns. It is characterized by the appearance of a mean flow in the azimuthal direction that breaks the reflection symmetry of the columns, but this solution preserves the  $Z_3$  invariance,  $Z_3$  being the cyclic group generated by the rotation  $R_{2\pi/3}$ .

Figure 3 shows the change in the structure of the col-

umns after the secondary bifurcation. Close to the bifurcation point, the pattern oscillates back and forth with a frequency given by the imaginary part of the eigenvalue whose real part becomes zero. The oscillation in the azimuthal direction can be appreciated in the shadowgraph of Fig. 3(a), which represents the evolution in time (y axis) of the temperature and its  $\theta$ -dependence (x axis). Clearly, the DRTW breaks the reflection symmetry with respect to vertical planes between the columns, but this periodic solution is a symmetric cycle, i.e., has the  $S$  symmetry

$$\Theta(x, \theta, t) = \Theta(x, 2\theta_0 - \theta, t + T/2),$$

$$f(x, t) = -f(x, t + T/2),$$

$$\psi(x, \theta, t) = -\psi(x, 2\theta_0 - \theta, t + T/2),$$

or in terms of the velocity field,  $(u, v)$ ,

$$u(x, \theta, t) = u(x, 2\theta_0 - \theta, t + T/2),$$

$$v(x, \theta, t) = -v(x, 2\theta_0 - \theta, t + T/2),$$

where  $T$  is the period of the wave. It loses the spatial reflection symmetry but gains this new spatio-temporal symmetry, and in this sense it can be said to maintain a  $D_3$  invariance. We will see later that the  $S$  symmetry is the clue for understanding the dynamics of the system at higher Rayleigh numbers. The new symmetry is also responsible for the period of the Nusselt number of the vacillating waves, defined in (6), to be half that of the velocity field. According to the symmetry relation, the temperature maintains the sign by a reflection and a half period shift in time. Then

$$\int_0^{2\pi} \partial_r \Theta(1, \theta, t) d\theta = \int_0^{2\pi} \partial_r \Theta(1, \theta, t + T/2) d\theta.$$

However, for the velocity field there is a change of sign in the relation, and  $\mathbf{v}(x, \theta, t) \neq \mathbf{v}(x, \theta, t + T/2)$ .

The new symmetry-breaking bifurcation can also be seen in Fig. 3(b), which shows the dependence of the azimuthal mean flow on the radial coordinate,  $x$ , in four time instants,  $t=0, T/4, T/2, 3T/4$ . After the bifurcation, the  $\theta$ -independent mode of  $v$  begins to contribute to the solution. As the area enclosed by each curve equals the instantaneous net mass flow, it can be inferred from the plot that there

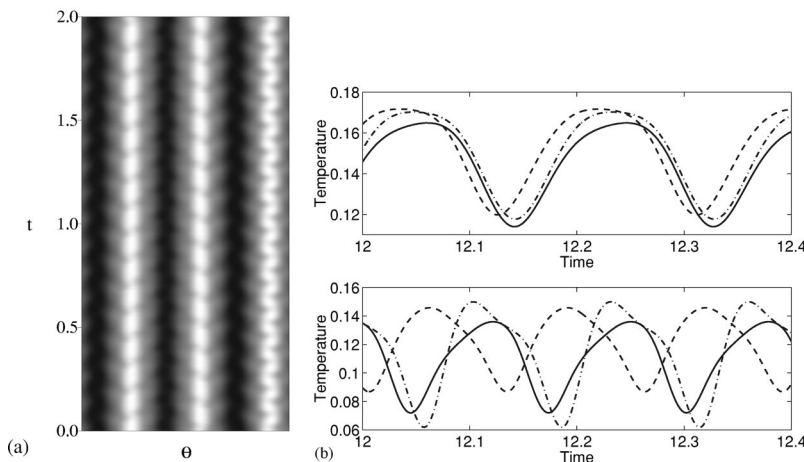


FIG. 4. (a) Shadowgraph showing the evolution of the temperature perturbation in time (y axis) at the radial midpoint of the annulus for a solution corresponding to  $Ra=12300$ . (b) Time dependence of the temperature showing the phase shift between the three points of the annulus of coordinates  $(L/2, \theta + 2\pi m/3)$ , with  $m=0,1,2$  and  $L$  the number of radial points.

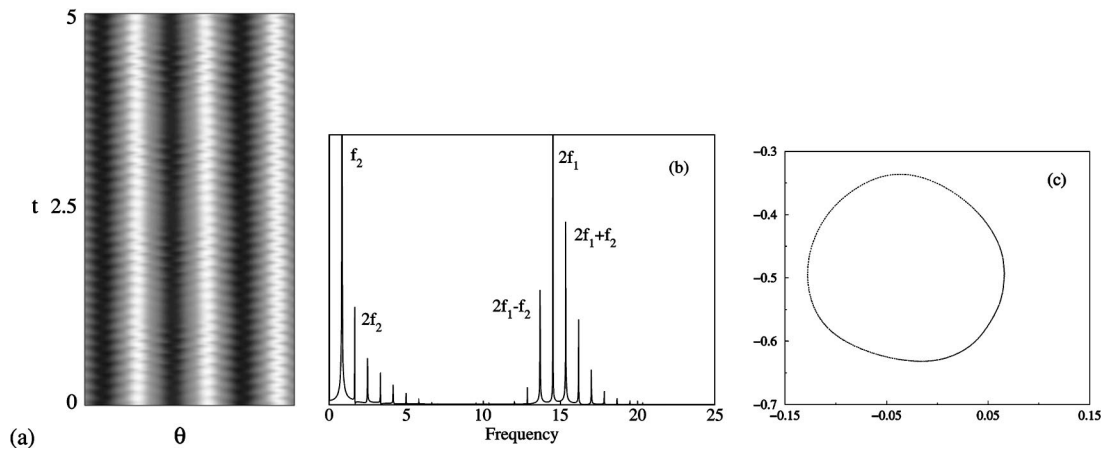


FIG. 5. Quasi-periodic solution at  $Ra=11\,500$  on the main  $n=3$  branch. (a) Shadowgraph showing the evolution of the temperature perturbation in time ( $y$  axis) in the radial midpoint of the annulus, (b) Fourier spectrum of the temporal series of the Nusselt number, and (c) Poincaré section displaying an odd versus an even azimuthal mode, in a fixed radial point.

exists an oscillatory mass transport in the azimuthal direction. That is, the instantaneous net mass flow is nonzero, though it vanishes when averaged in a whole period. The value of the frequency grows as the Rayleigh number increases. Just at the bifurcation point, for a Rayleigh number  $Ra_c^4=4114$ , the frequency is  $f=3.74$ , while for a Rayleigh number  $Ra=6500$ , the Fourier spectrum shows that the solution still remains periodic, the frequency of oscillation being  $f=5.15$ .

Between  $Ra=6950$  and  $Ra=7000$  a tertiary spatial subharmonic bifurcation, which breaks the last spatial symmetry of the solutions, is identified in the system. The symmetry breaking implies that the modes  $n \neq 3$  start to grow. We have carefully checked that at the tertiary bifurcation there is no new frequency appearing in the Fourier spectra of the time series after the transition, so the new solution remains periodic. This fact agrees with bifurcation theory, which establishes that in a codimension one bifurcation of a symmetric cycle only the multipliers  $\mu=1$  and  $\mu=e^{\pm i\theta_0}$  of the associated Poincaré map can appear.<sup>26</sup> In our case the unit circle is crossed by the real multiplier. Figure 4(a) is a shadowgraph of the temperature of the new periodic orbit very far from transition, for  $Ra=12\,300$ . It is plotted at a fixed radius, and clearly shows that, as a result, the spatial discrete rotational invariance of the columns is broken, but the symmetry  $S$  is preserved. The new pattern of convection consists of three oscillating columns like those in the DRTW, but with different waveforms, amplitudes, and phases. The waveform is nearly the same in two of them, but the third one clearly differs from the others. Figure 4(b) shows that three angularly equally spaced points, each in a column, which before the bifurcation were oscillating in phase, begin to oscillate out of phase. The phase shift increases with the Rayleigh number more for one of the columns than for the other two, which remain nearly in phase, and, in addition, the shape of one of the columns changes substantially. These are the reasons why in the shadowgraph it seems that they oscillate with a different period. A similar cell pattern can be found when a fixed point bifurcates with trihedral  $D_3$  symmetry.<sup>27</sup>

When  $Ra \approx 12\,330$ , the system undergoes a subcritical

Neimark–Sacker bifurcation. In the shadowgraph of Fig. 5(a) one may see what this solution looks like. Its Poincaré section [Fig. 5(c)] shows clearly that an invariant two-dimensional torus appears. The turning point is at  $Ra \approx 11\,425$ . From the Fourier spectrum of the time series of the Nusselt number, included in Fig. 5(b), it can be seen that the new frequency in the system is very small,  $f_2=0.815$ , in comparison with the value of the main one,  $f_1=7.26$ . It is important to point out that, in this spectrum, the frequency,  $2f_1$ , appears as a main frequency because the quasi-periodic solution bifurcates from an  $S$  cycle, and the Rayleigh number must be increased further for  $f_1$  to become apparent. Thus, near the bifurcation point, the main frequency of the Nusselt number remains twice the main frequency of the velocity field.

The quasi-periodic solution turns out to be stable in a small interval of the control parameter. A moderate increment in the Rayleigh number produces a great change in the dynamics of the system, the solution being already chaotic for a Rayleigh number  $Ra=12\,000$ . This can be observed in Fig. 6, where the Fourier spectrum of the time series of the Nusselt number, at  $Ra=13\,000$ , is plotted. They clearly indicate the appearance of a wide band of frequencies, now including the  $f_1$  frequency, in the solution. Temporal chaos is thus reached by a Ruelle–Takens via, after three time-

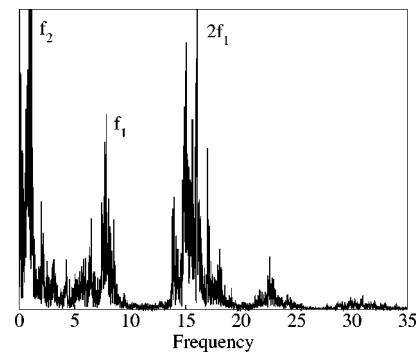


FIG. 6. Fourier spectrum of the temporal series of the Nusselt number. The solution corresponds to  $Ra=13\,000$  on the main  $n=3$  branch.

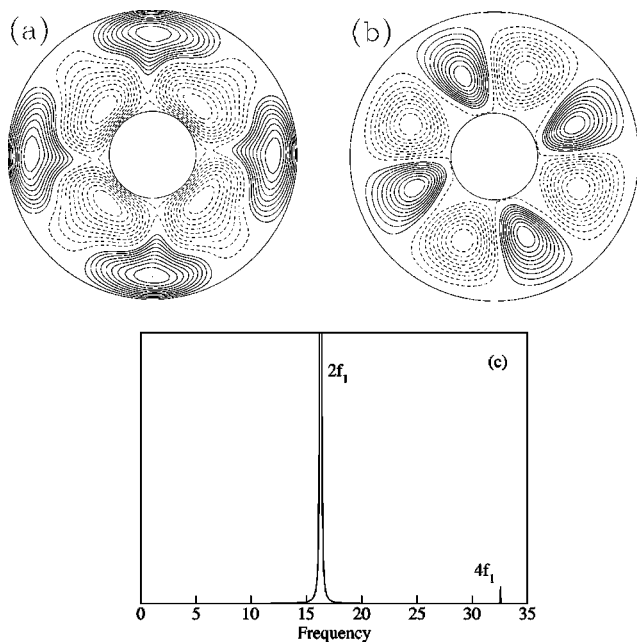


FIG. 7. For the pure  $n=4$  DRTW at  $Ra=14\,000$ , (a) contour plots of the perturbation of the temperature, (b) of the streamfunction, and (c) Fourier spectrum of the temporal series of the Nusselt number. As in the  $n=3$  DRTW, the main frequency for the velocity field is  $f_1$ .

dependent, but four symmetry-breaking, bifurcations. Without any remaining symmetry the fifth one leads to chaos. It will be seen that the aperiodic solutions maintain the three columnar structure until they reach much higher Rayleigh numbers.

### B. Nonlinear solutions with basic dominant wavenumber $n=4$

We have seen in Sec. III that the  $N4$  branch is stabilized at  $Ra_c^{12}=4779$  giving rise to steady columns of basic wavenumber  $n=4$ , which have the same symmetry properties as the steady  $n=3$  columns. The  $n=4$  steady stable solutions coexist with the DRTW of basic wavenumber  $n=3$  until  $Ra_c \approx 6897$ , where they undergo a Hopf bifurcation that keeps the spatial periodicity. Both the  $n=3$  and  $n=4$  steady solutions have the same symmetry properties, and the new pattern of convection is again a DRTW, like that of Fig. 3(a), but with four columns and a frequency  $f_1=5.46$ , confirmed also by the eigenvalues  $\lambda_I = \pm 34.3$  that cross the imaginary axis, in the linear stability problem. From  $Ra_c=6897$ , the new stable  $n=4$  DRTW coexists with the periodic solutions described in Sec. IV A until  $Ra \approx 10\,500$ . Preliminary calculations of the stability of the periodic orbit, and also enormously long transients of the time-dependent codes, indicate that at this point there exists a pitchfork bifurcation of periodic orbits that, ultimately, give rise to branches of mixed DRTW. In spite of the symmetry-breaking, the contour plots of all these waves are very similar because the amplitudes of the growing  $n=2$  and after  $n=1,3$  modes are small. When the mixed DRTW bifurcates, we have not found any stable branch of new solutions locally connected with either the mixed DRTW or the pure DRTW branches. We suspect that high codimension bifurcations take place in the vicinity of

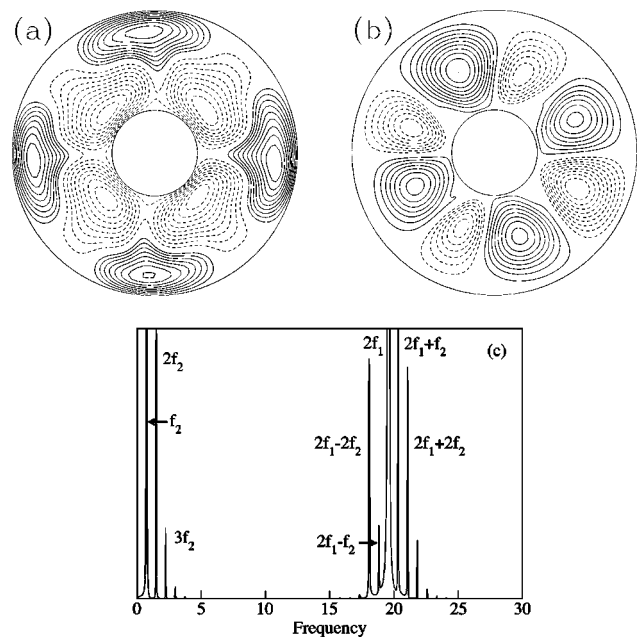


FIG. 8. For the quasi-periodic solution at  $Ra=18\,900$ , (a) contour plots of the perturbation of the temperature, (b) of the streamfunction, and (c) Fourier spectrum of the temporal series of the Nusselt number. As in the  $n=3$  quasi-periodic solution, the main frequency of the solution is  $f_1$ .

the points where the solutions are lost. The  $n=4$  DRTW solutions remain almost stable up to  $Ra \approx 14\,800$ , because the simple multiplier that first crosses the unit circle remains very close to 1.0.

For  $Ra > 18\,400$ , two branches of  $R$ -conjugate quasi-periodic solutions with dominant wavenumber  $n=4$  and second frequency  $f_2=0.83$  (VP) at  $Ra=18\,500$  have been detected independently, by changing the integration initial conditions. Because  $f_2 \ll f_1$ , it is easy to check that one of them can be obtained by applying a reflection symmetry to the other. In this case we have found that the reflection is through the  $\theta_0 \approx -\pi/4$  plane. These solutions are mixed modulated direction reversing traveling waves (mixed-MDRTW), whose period  $T_2$  and maximum amplitude increase with  $Ra$  until  $Ra \approx 20\,000$ , where they seem to saturate. The comparison of the contour plots and Fourier spectra of the  $n=4$  pure and mixed DRTW and those of the quasi-periodic solution leads us to believe that this scenario is organized by later bifurcations of the DRTW. See Figs. 7(a)–7(c) and Figs. 8(a)–8(c) as examples. On one hand, we have checked that the contour plots of the variables at any instant of time are very similar (except for the phase of the wave) and, on the other hand, that the main frequency  $f_1$  of Fig. 8(c) almost corresponds to a continuous increase of the frequency of the DRTW, shown in Fig. 7(c), due to the increase of the Rayleigh number. To confirm this point with a time evolution code, we have taken as initial condition for a fixed Rayleigh number, where the solution is unstable, the preceding solution before it stabilizes, and we have integrated the equations until only the dominant  $n=4$  modes and its harmonics saturate, but the other modes are still negligible. Because the transients are very long, we can calculate the frequency of the unstable solutions we are following. For

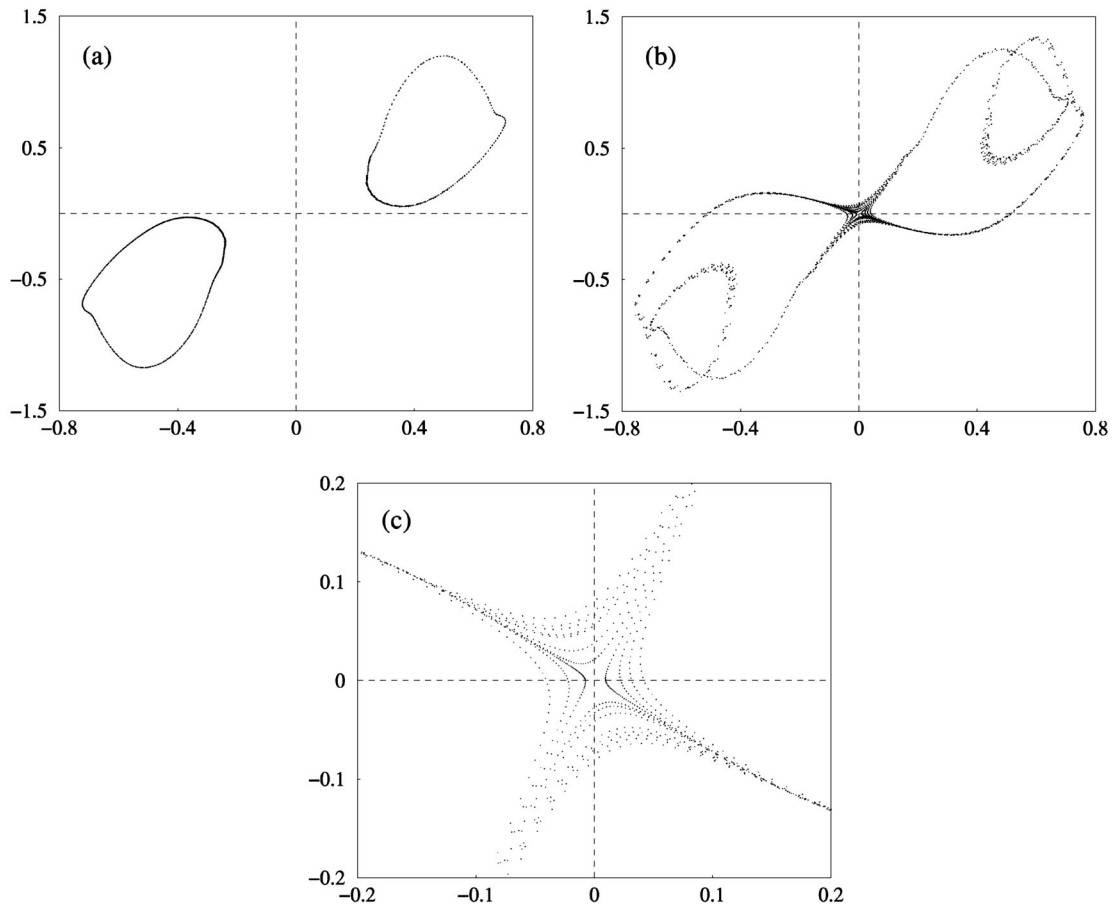


FIG. 9. (a) and (b) Poincaré sections of two  $R$ -conjugate tori and of the near homoclinic toroidal structure at  $Ra=20\,150$ , respectively, and (c) detail of (b) near the origin. An odd mode of the azimuthal component of the velocity vs an odd mode of the radial component of the velocity is represented, for a fixed radial point.

example, at  $Ra=14\,000$ ,  $16\,500$ , and  $Ra=18\,000$  the frequencies are  $f_1=8.15$ ,  $8.81$ , and  $9.25$ , respectively, while for the quasi-periodic stable solutions it is  $f_1=9.79$  for  $Ra=18\,900$ . Both facts indicate that these branches are related in some way with the  $n=4$  DRTW. Figure 9(a) shows the Poincaré section of the above-mentioned  $R$ -conjugate tori at  $Ra=20\,150$ . At the same  $Ra$  we have also found (with the two time evolution codes) a solution whose Poincaré section, which is represented in Fig. 9(b), is a *reflection-symmetric figure-eight homoclinic attractor*. We plot odd modes of the components of the velocity field, so that the unstable DRTW cross the hyper-plane at the origin. At first sight, it would seem that the figure-eight structure appears in a gluing bifurcation of the two  $R$ -conjugate tori, but they coexist, maintaining their amplitude, until  $Ra\approx 20\,200$ , where the pair of quasi-periodic solutions disappears. We include in Fig. 9(c) a blow up of the return map of Fig. 9(b) near the origin. From these figures it is clear that the system spends a lot of time near the DRTW and escapes very fast, jumping randomly from one side to the other [see also Figs. 10(a) and 10(b)]. The small difference that can be appreciated in the tori of Fig. 9(a) is due to the rotational invariance of the system. In fact, there exists an infinite number of  $R$ -conjugate tori and also homoclinic attractors that only differ in the azimuthal orientation of the columns; so generically, with random ini-

tial conditions, the solutions we found are rotated in an arbitrary phase (in the case of the figure, a small one).

From  $Ra\approx 20\,070$ , the dynamics is very complex. We have found several stable quasi-periodic solutions of different periods and symmetries in a small region of the parameter space. In Figs. 10(a) and 10(b) we show a sample of the type of flows found. They correspond to the time series of the Nusselt number and to the real part of the  $n=1$  mode of the radial velocity, respectively, for different values of the Rayleigh number. The upper two are quasi-periodic solutions of different amplitude and radial component velocity sign, like those of Fig. 9(a). The next is a chaotic solution, like that of Fig. 9(b). After the random switches, the flow relaminarizes giving rise to  $R$ -invariant quasi-periodic solutions whose long periods, in Fig. 10, quadruples that of a single of the  $R$ -conjugate torus. For  $Ra\approx 20\,900$  there is no doubt that at least one quasi-periodic orbit homoclinic to the pure  $n=4$  DRTW is formed. As can be seen in the last but one row of Figs. 10(a) and 10(b), the  $n=1$  azimuthal mode (in fact all the  $n\neq 4$  modes) vanishes during the long periods where the flow behaves like the periodic unstable DRTW at the origin. This is an indication that the big  $R$ -invariant torus nearly intersects the origin. Furthermore, there are some signs that other pairs of  $R$ -conjugate solutions glue to form homoclinic

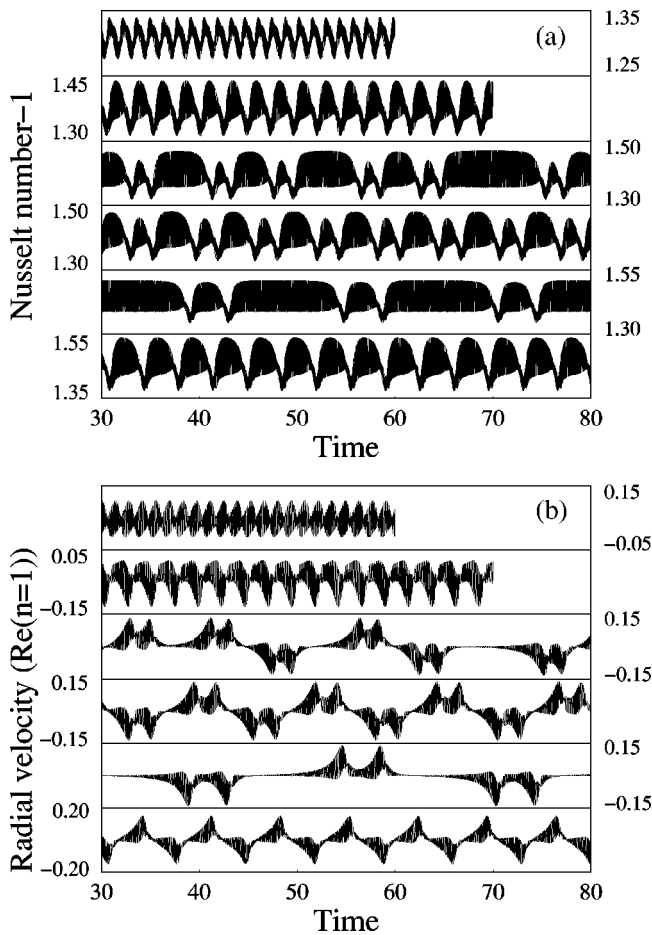


FIG. 10. Time series of (a) the Nusselt number and (b) the real part of the  $n=1$  Fourier coefficient of the radial velocity at a fixed radial point. The solutions from top to bottom correspond to  $Ra=19\,000$ ,  $Ra=20\,000$ ,  $Ra=20\,200$ ,  $Ra=20\,500$ ,  $Ra=20\,900$ , and  $Ra=22\,000$ .

quasi-periodic orbits, at almost the same value of the Rayleigh number. The last row of the same figure corresponds to a quasi-periodic orbit whose period is double that of the torus of Fig. 9(a). All these tori behave like MDRTW.

If we try to follow the branch of quasi-periodic solutions below  $Ra \approx 18\,250$  by decreasing the Rayleigh number, the system evolves to the chaotic solution with the above-mentioned basic azimuthal wavenumber  $n=3$ .

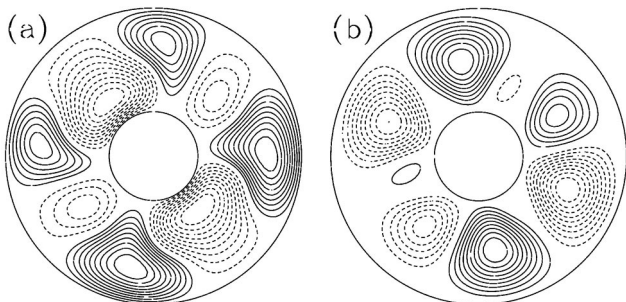


FIG. 11. Contour plots of the mixed-mode steady column (a) of the perturbation of the temperature and (b) of the streamfunction. The solution corresponds to  $Ra=5200$ .

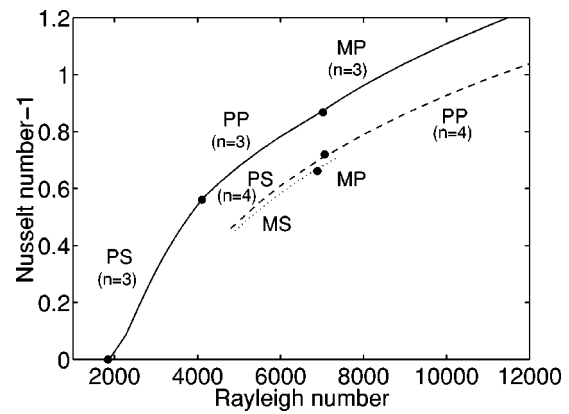


FIG. 12. Nusselt number as a function of the Rayleigh number for steady state and periodic solutions. The solid, dashed, and dotted lines correspond, respectively, to the basic  $n=3$ ,  $n=4$ , and the mixed stable solutions. For the time-dependent solutions we have plotted the averaged period. The labels stand for: PS pure steady, PP pure periodic, MS mixed steady, MP mixed periodic solutions.

### C. Nonlinear solutions on the mixed-mode branch

For a Rayleigh number  $Ra \approx 4850$ , we have found another branch of mixed-mode steady stable columns, which is not connected with the conduction state. The existence of this branch is in agreement with a recent work,<sup>17</sup> in which two-dimensional non-Boussinesq convection is analyzed in the case of a strong 1:2 spatial resonance. According to these authors, in a saddle node bifurcation point the solution ceases to exist. In our case, by decreasing the  $Ra$  below  $Ra \approx 4850$ , there is a transition to the main  $n=3$  branch of solutions. The structure of the new solution is shown in Fig. 11. As in the case of the mixed-mode branch  $N2$  of Fig. 1, the solutions keep a spatial reflection symmetry, so their group of symmetry is  $Z_2$ . The vertical plane of symmetry crosses the temperature contour plot through the middle of the big negative temperature vortex.

Between  $Ra=6800$  and  $Ra=7150$ , the system undergoes a Hopf bifurcation that breaks the spatial reflection symmetry,  $R$ , of the steady solutions, giving rise to a stable mixed DRTW, which has a weak azimuthal mean flow. The new solution is a symmetric cycle, then the main frequency of the Fourier spectrum of the Nusselt number is again twice that of the velocity field  $f_1$ . At  $Ra=7150$ , its frequency is  $f_1=5.80$ , which is very similar to that found for the  $n=4$  DRTW. Figure 12 displays the dependence of this number, averaged in time for the periodic solutions, on the Rayleigh number. The solid and dashed lines correspond, respectively, to the basic  $n=3$ ,  $n=4$  solutions found by increasing the Rayleigh number. The dotted lines are the mixed stable solutions that also coexist with the others. It is clear that the convection is more efficient if the  $n=3$  column is selected, while for the other two patterns it is very similar. After the Hopf bifurcation, there is a significant decrease in the slope of the curves. This slowing down in the efficiency of the radial heat transport is caused by the appearance of the oscillatory mass flow in the azimuthal direction that increases the kinetic energy of the flow. Therefore, the bigger the mean

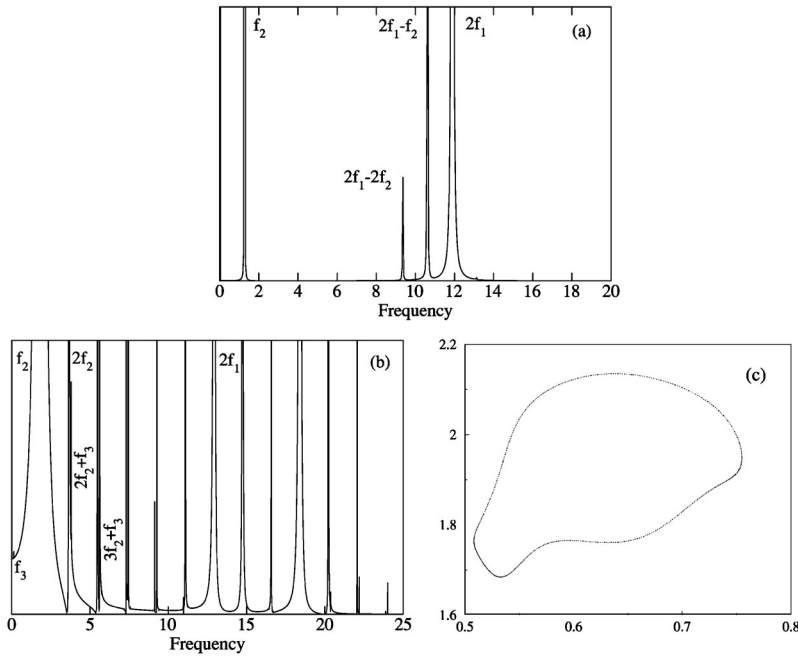


FIG. 13. (a) Fourier spectrum of the temporal series of the Nusselt number for the two-frequency quasi-periodic solution on the mixed-mode branch at  $Ra = 7450$  and (b) same plot for the stable three-frequency quasi-periodic solution at  $Ra=15\,000$ . As in the  $n=3$  DRTW, the main frequency for the velocity field is  $f_1$ .

flow the larger the decrease in the slope of the Nusselt number.

The periodic orbit turns out to be stable in a very short range of Rayleigh numbers. At  $Ra \approx 7400$ , the system undergoes a Neimark–Sacker bifurcation, giving rise to quasi-periodic solutions that are mixed-MDRTW. So, at a fixed instant, the contour plots of the quasi-periodic solutions look like those of Fig. 11. The Fourier spectrum of Fig. 13(a) corresponds to a solution at  $Ra = 7450$ , the second frequency being  $f_2 = 1.27$ . At  $Ra = 15\,000$  a solution with a small third frequency  $f_3 = 0.13$  is found. The peak of this frequency can be seen in Fig. 13(b) and, moreover, linearly combined with other peaks. However, its Poincaré section [Fig. 13(c)] re-

veals that the flow is still a two-tori. This fact, together with the long new period  $f_3^{-1}$ , indicate that the system is crossing a region of phase locking in the parameter space. This solution is stable at least up to  $Ra = 18\,000$  and when it becomes chaotic, a broadband of frequencies appears in the spectrum.

### V. DISCUSSION

To clarify the scenario presented in the preceding sections, a self-explanatory sketch of the sequence of bifurcations leading to stable flows up to  $Ra = 20\,150$  is plotted in Fig. 14. As usual, dashed and solid lines refer to unstable and stable solutions, respectively. The branches not leading to stabilization (as far as our calculations reveal) are cut near the bifurcation point and only branches that are relevant to the later global dynamics at higher Rayleigh numbers have been prolonged. Despite the complexity of the diagram, the existence of other branches of stable solutions in this region of the parameter space cannot be ruled out. We hope to be able to obtain detailed results about the stability of the periodic orbits in the near future, and therefore clarify the connection between the mixed DRTW branch, which reaches the highest Rayleigh numbers, and the quasi-periodic solutions of basic azimuthal wavenumber  $n = 4$ .

As far as the influence of the reflection symmetry is concerned, we have found two types of nonlinear dynamics. The first one is not affected by the symmetries, and corresponds to the behavior of the main branches of solutions of basic azimuthal wavenumber  $n = 3$ . The onset of temporal chaotic dynamics takes place with the appearance of a third time-dependent bifurcation that introduces a new incommensurate frequency. In spite of the existence of a pitchfork bifurcation of periodic orbits between the first periodic and the quasi-periodic regimes, the sequence can be considered an example of the Ruelle and Takens theory. This type of transition was first observed in a Taylor–Couette apparatus<sup>28</sup> and

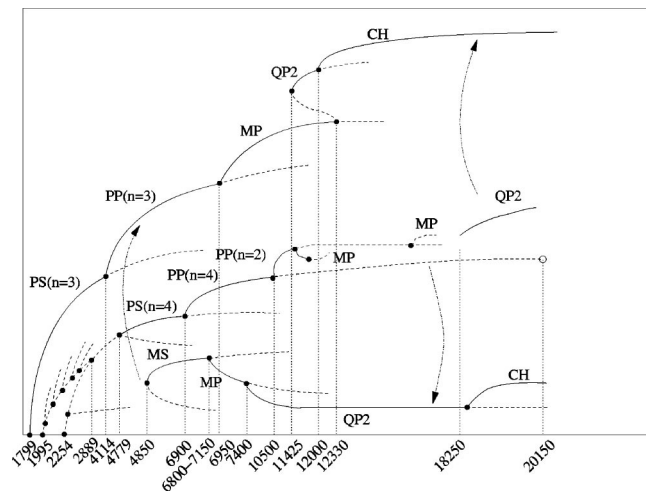


FIG. 14. Sketch of the sequence of bifurcations found in the two-dimensional annular geometry. Any type of solutions are represented by lines. As usual, dashed for the unstable flows and solid for the stable, respectively. The labels stand for: PS pure steady, PP pure periodic, MS mixed steady, MP mixed periodic, QP2 two-frequency quasi-periodic, and CH chaotic solutions.

since then has been observed in numerous experiments of thermal convection in rectangular boxes and in other dynamical systems with different symmetries. It is an universal route to chaos, and experiments confirm that is independent of the symmetry group of the system. Thus we must conclude that  $O(2)$  symmetry would not modify the temporal dynamics of the  $n=3$  dominant thermal columns. In contrast, the nonlinear dynamics of the solutions of dominant wavenumber  $n=4$  depends on the reflection symmetry, locally for the steady and periodic solutions and globally for those quasi-periodic. The spatial interaction between the modes with wavenumbers  $n=2$  and  $n=4$  that we have found is an example of a spatial 1:2 resonance, in which modes with wavenumbers  $n$  and  $2n$  in the periodic direction interact nonlinearly. The 1:2 spatial resonance in systems with  $O(2)$  symmetry was first studied by several authors.<sup>29,30</sup> Some aspects of the dynamics predicted by the normal form equations are reproduced here, although slightly modified by the initial existence of the stable  $n=3$  branch. The presence of wavenumber gaps in which no steady solutions with a given wavenumber exist is a typical feature of this resonance. This is what happens in the range of Rayleigh numbers  $2889 < Ra < 4779$ , where the  $n=2$  solution disappears. The existence of traveling waves bifurcating from the mixed  $n=2,4$  mode, which correspond to the bifurcation point at  $Ra_c^5 = 2478$  in our case, is also a characteristic of this resonance. Moreover, in agreement with Ref. 17, the third stable mixed-mode branch disconnected from the conduction state completes our 1:2 standard resonant bifurcation diagram. The transition to turbulence through quasi-periodic states and the phase locking phenomenon with three frequencies in Rayleigh–Bénard convection have also been known for a long time,<sup>31,32</sup> but are not easy to observe in laboratory experiments. Our results confirm the existence of such regimes in natural thermal convection, but a detailed study of the transition to temporal chaotic flows from three-tori is outside the scope of this paper. In any case, we would like to point out that we have also found the  $R$  and  $R_\theta$ -symmetric branches of solutions, but no hint that it could affect the complex global dynamics at higher Rayleigh numbers.

The quasi-periodic solutions and the homoclinic attractors found at  $Ra \approx 20\,150$  and  $Ra \approx 20\,900$  are not directly related with the standard interaction of the  $n=2$  and  $n=4$  azimuthal modes; i.e., they have no direct relation to the tori and heteroclinic cycles<sup>16</sup> found from the normal form equations of the 1:2 resonance. In this reduced system, they are always found below the point where the stabilization of the  $n=4$  steady column takes place. The following dynamics is globally organized by the  $n=4$  periodic orbit and two reflection-symmetric time-dependent branches of solutions. In this sense, it would also be characteristic of  $Z_2$  symmetric systems. See for instance, Lopez and Marques<sup>33</sup> results for a periodically forced Taylor–Couette apparatus. The global dynamics described in this paper is also present in other systems with discrete symmetry groups. Most of the solutions we found are in consonance with the results of Armbruster *et al.*<sup>34</sup> The authors analyzed the sequence of global bifurcations for partial differential equations with  $D_4$  symmetry. They use a Karhunen–Loève analysis to identify the struc-

tures in phase space that generate the behavior of low Reynolds number Kolmogorov flow, in a two-dimensional periodic domain. Our results are in agreement with the existence of a gluing bifurcation of limit cycles (four in their case) that generate a  $D_4$ -invariant attractor. Gluing bifurcations are the symmetry-increasing mechanism that probably generate an inverse period-doubling cascade leading to the chaotic attractor at  $Ra \approx 20\,150$ . It is difficult to explore a large range of the parameter space for quasi-periodic solutions in detail, but this mechanism of period-doubling in Rayleigh–Bénard convection has already been carefully described by Massaguer *et al.*<sup>35</sup> for a subharmonic period-doubling cascade of periodic orbits. They found that the scenario was generated by a sequence of gluing bifurcations between asymmetrical orbits, which gave rise to symmetrical orbits of double period and, subsequently, pitchfork bifurcations of the new periodic orbits return to the asymmetrical situation. It is important to notice that global bifurcations involving solutions related by the symmetries of the problem require the real existence of these symmetries. It is not enough that a single solution recovers locally a symmetry under special circumstances. Thus, in the three-dimensional problem, even if the boundary layers remains laminar and attached to the lids of the annulus, and the fluid remains nearly two-dimensional because of rotation, the dynamics of the almost  $n=4$  thermal columns should be completely different to that described here.

Finally, we would like to point out that although pure steady columns, forced by a radial temperature gradient, cannot be experimentally observed on the Earth's surface, because of vertical gravity, there are some old<sup>36</sup> and new experiments designed to be carried out in radial gravity conditions in a space station. The most recent of these is currently being designed at the University of Colorado (see <http://nimbus.colorado.edu/hart/science.htm>) in order to study shear flow instabilities in a ferromagnetic Taylor–Couette apparatus, whose walls are maintained at different temperatures. We trust that our results contribute to a general understanding of the influence of the radial gravity on convective systems with curvature.

## ACKNOWLEDGMENT

This work was supported by MCYT under Grant No. BFM2001-2336.

<sup>1</sup>F.H. Busse and C.R. Carrigan, "Convection induced by centrifugal buoyancy," *J. Fluid Mech.* **62**, 579 (1974).

<sup>2</sup>M.A. Azouni, E.W. Bolton, and F.H. Busse, "Convection driven by centrifugal buoyancy in a rotating annulus," *Geophys. Astrophys. Fluid Dyn.* **34**, 301 (1986).

<sup>3</sup>F.H. Busse and A.C. Or, "Convection in a rotating cylindrical annulus: Thermal Rossby waves," *J. Fluid Mech.* **166**, 173 (1986).

<sup>4</sup>A.C. Or and F.H. Busse, "Convection in a rotating cylindrical annulus. Part 2. Transitions to asymmetric and vacillating flow," *J. Fluid Mech.* **174**, 313 (1987).

<sup>5</sup>R.-Q. Lin, F.H. Busse, and M. Ghil, "Transition to two-dimensional turbulent convection in a rapidly-rotating annulus," *Geophys. Astrophys. Fluid Dyn.* **45**, 131 (1989).

<sup>6</sup>R.-Q. Lin, "Double column instabilities in the barotropic annulus," *Geophys. Astrophys. Fluid Dyn.* **54**, 161 (1990).

<sup>7</sup>A.C. Or, "Chaotic transitions of convection rolls in a rapidly rotating annulus," *J. Fluid Mech.* **261**, 1 (1994).

- <sup>8</sup>N.H. Brummell and J.E. Hart, "High Rayleigh number  $\beta$ -convection," *Geophys. Astrophys. Fluid Dyn.* **68**, 85 (1993).
- <sup>9</sup>D. Pino, I. Mercader, and M. Net, "Thermal and inertial modes of convection in a rapidly rotating annulus," *Phys. Rev. E* **61**, 1507 (2000).
- <sup>10</sup>D. Pino, M. Net, J. Sánchez, and I. Mercader, "Thermal Rossby waves in a rotating annulus," *Phys. Rev. E* **63**, 056312 (2001).
- <sup>11</sup>H.F. Goldstein, E. Knobloch, I. Mercader, and M. Net, "Convection in a rotating cylinder. Part I. Linear theory for moderate Prandtl numbers," *J. Fluid Mech.* **248**, 583 (1993).
- <sup>12</sup>A. Alonso, M. Net, and E. Knobloch, "On the transition to columnar convection," *Phys. Fluids* **7**, 935 (1995).
- <sup>13</sup>K. Zhang and G.T. Greed, "Convection in rotating annulus: An asymptotic theory and numerical solutions," *Phys. Fluids* **10**, 2396 (1998).
- <sup>14</sup>A. Alonso, M. Net, I. Mercader, and E. Knobloch, "Onset of convection in a rotating annulus with radial gravity and heating," *Fluid Dyn. Res.* **24**, 133 (1999).
- <sup>15</sup>G.T. Greed and K. Zhang, "Two- and three-dimensional linear convection in a rotating annulus," *Geophys. Astrophys. Fluid Dyn.* **82**, 23 (1996).
- <sup>16</sup>S.M. Cox, "Mode interactions in Rayleigh–Bénard convection," *Physica D* **95**, 50 (1996).
- <sup>17</sup>G. Manogg and P. Metzener, "Strong resonance in two-dimensional non-Boussinesq convection," *Phys. Fluids* **6**, 2944 (1994).
- <sup>18</sup>J. Mizushima and K. Fujimura, "Higher harmonic resonance of two-dimensional disturbances in Rayleigh–Bénard convection," *J. Fluid Mech.* **234**, 651 (1992).
- <sup>19</sup>M. Golubitsky and D.G. Schaeffer, *Singularities and Groups in Bifurcation Theory* (Springer, New York, 1985), Vol. I.
- <sup>20</sup>E. Knobloch, "Symmetry and instability in rotating hydrodynamic and magnetohydrodynamic flows," *Phys. Fluids* **8**, 1446 (1996).
- <sup>21</sup>E.S. Landsberg and E. Knobloch, "Direction-reversing travelling waves," *Phys. Lett. A* **159**, 17 (1991).
- <sup>22</sup>Z.A. Daya, V.B. Deyirmenjian, S.W. Morris, and J.R. de Bruyn, "Annular electroconvection with shear," *Phys. Rev. Lett.* **80**, 964 (1998).
- <sup>23</sup>Z.A. Daya, V.B. Deyirmenjian, and S.W. Morris, "Bifurcations in annular electroconvection with imposed shear," *Phys. Rev. E* **64**, 036212 (2001).
- <sup>24</sup>A. Alonso, M. Net, and J. Sánchez, "Spatially resonant interactions in annular convection," *Proceedings of the Conference on Bifurcations Symmetry and Patterns* (Birkhäuser, Boston, in press).
- <sup>25</sup>A. Alonso, J. Sánchez, and M. Net, "Transition to temporal chaos in an  $O(2)$ -symmetric convective system for low Prandtl numbers," *Prog. Theor. Phys. Suppl.* **139**, 315 (2000).
- <sup>26</sup>Y.A. Kuznetsov, *Elements of Applied Bifurcation Theory* (Springer, New York, 1998).
- <sup>27</sup>M. Golubitsky, I. Stewart and D.G. Schaeffer, *Singularities and Groups in Bifurcation Theory* (Springer, New York, 1985), Vol. 2.
- <sup>28</sup>J.P. Gollub and H.L. Swinney, "Onset of turbulence in a rotating fluid," *Phys. Rev. Lett.* **35**, 927 (1975).
- <sup>29</sup>G. Dangelmayr, "Steady-state mode interactions in the presence of  $O(2)$ -symmetry," *Dyn. Stab. Syst.* **1**, 159 (1986).
- <sup>30</sup>M.R.E. Proctor and C.A. Jones, "The interaction of two spatially resonant patterns in thermal convection," *J. Fluid Mech.* **188**, 301 (1988).
- <sup>31</sup>J. Maurer and A. Libchaber, "Effect of the Prandtl number on the onset of the turbulence in liquid  $^4\text{He}$ ," *J. Phys. (France) Lett.* **41**, L-515 (1980).
- <sup>32</sup>J.P. Gollub and S.V. Benson, "Many routes to turbulent convection," *J. Fluid Mech.* **100**, 449 (1980).
- <sup>33</sup>J.M. Lopez and F. Marques, "Dynamics of three-tori in a periodically forced Navier–Stokes flow," *Phys. Rev. Lett.* **85**, 972 (2000).
- <sup>34</sup>D. Armbruster, B. Nicolaenko, N. Smaoui, and P. Chossat, "Symmetries and dynamics for 2-D Navier–Stokes flow," *Physica D* **95**, 81 (1996).
- <sup>35</sup>J.M. Massaguer, I. Mercader, and M. Net, "Nonlinear dynamics of vertical vorticity in low-Prandtl-number thermal convection," *J. Fluid Mech.* **214**, 579 (1990).
- <sup>36</sup>J.E. Hart, G.A. Glatzmaier, and J. Toomre, "Space-laboratory and numerical simulations of thermal convection in a rotating hemispherical shell with radial gravity," *J. Fluid Mech.* **173**, 519 (1986).